

Orbital Parameters of Infalling Dark Matter Substructures

A. J. Benson

Department of Physics, University of Oxford, Keble Road, Oxford OX1 3RH, United Kingdom (e-mail: abenson@astro.ox.ac.uk)

28 August 2018

ABSTRACT

We present distributions of the orbital parameters of dark matter substructures at the time of merging into their host halo. Accurate knowledge of the orbits of dark matter substructures is a crucial input to studies which aim to assess the effects of the cluster environment on galaxies, the heating of galaxy disks and many other topics. Orbits are measured for satellites in a large number of N-body simulations. We focus on the distribution of radial and tangential velocities, but consider also distributions of orbital eccentricity and semi-major axis. We show that the distribution of radial and tangential velocities has a simple form and provide a fitting formula for this distribution. We also search for possible correlations between the infall directions of pairs of satellites, finding evidence for positive correlation at small angular separations as expected if some infall occurs along filaments. We also find (weak) evidence for correlations between the direction of the infall and infall velocity and the spin of the host halo.

Key words: cosmology: theory - dark matter - galaxies: halos

1 INTRODUCTION

In currently favoured cosmological models, dark matter halos grow via the merging together of smaller systems, leading to an ever-growing hierarchy of halos. Recent numerical simulations have demonstrated that the remnants of pre-existing dark matter halos which merged to become part of a larger system (the “host”) can survive for significant periods of time within the larger system (Moore et al. 1999; Klypin et al. 1998). These subhalos orbit around in the potential of the host gradually losing mass via tidal forces and spiralling in to ever smaller radii due to dynamical friction. These substructures (or at least some subset of them) are presumably the abodes of satellite galaxies, such as those found in the Local Group, and of the majority of cluster galaxies.

This substructure has attracted a great deal of interest since its discovery. Observational tests for its presence, though not yet conclusive, are in good agreement with the theoretical expectations (Metcalf & Madau 2001; Chiba 2002; Dalal & Kochanek 2002). There has been much work conducted in which the distribution and properties of substructures, their effects on galaxy disks and so on were examined (Ghigna et al. 1998; Tormen, Diaferio & Syer 1998; van den Bosch et al. 1999; Zhang et al. 2002; Benson et al. 2004; Gao et al. 2004; Diemand, Moore & Stadel 2004). While the orbital parameters of substructures have been measured in the past this measurement has often been at the end point of the substructure evolution (i.e. at the present day) when significant dynamical evolution in the orbital parameters is

expected (e.g. Ghigna et al. 1998). Exceptions to this are the works of Tormen (1997), Vitvitska et al. (2002) and Khochfar & Burkert (2004). Tormen (1997) and Khochfar & Burkert (2004) both identified progenitors of halos in their N-body simulations and measured the orbital parameters of them, while Vitvitska et al. (2002) searched for pairs of halos about to merge and measured the orbital parameters of these. These works have typically made use of rather small samples of orbits and (perhaps consequently) have been unable to fully characterise the two dimensional distribution of orbital parameters needed to construct realistic orbits.

The distribution of initial orbital parameters of substructure halos at the time of merging into the host system is a particularly interesting property as it represents the initial conditions which determine the later evolution of the substructure within the host. The effectiveness of many processes invoked to explain the morphological transformation of galaxies in clusters (e.g. ram pressure stripping, tidal mass loss, galaxy harassment, etc.) depend crucially on the nature of the galaxy orbit (see, for example, Moore, Lake & Katz 1998; Abadi, Bower & Navarro 2000). The distribution of orbits will also determine the rate of galaxy mergers and therefore the degree of heating and rate of morphological transformation experienced by galaxy disks. Taking a more practical point of view, recent semi-analytic models of satellite halo orbits (Benson et al. 2002; Taylor & Babul 2004) have been able to follow the orbital evolution of satellites quite accurately, but these models are only as good as

arXiv:astro-ph/0407428v1 20 Jul 2004

their initial conditions which, until now, have been known only rather poorly.

In this work, we quantify the distribution of orbital parameters for dark matter halos at the point of merging with their host (i.e. we proceed in a similar way as did Vitvitska et al. 2002). We measure this distribution in a large number of N-body simulations to attain high statistical precision and to facilitate checks of our techniques and tests for variations of the distribution of orbital parameters with variables such as redshift, halo mass etc. While we will present distributions of orbital eccentricity and semi-major axis, our focus is on distributions of radial and tangential velocities, which we find are more practical when dealing with orbits in non-spherical systems in which dynamical friction is at work¹. We also examine the distribution of infalling substructures as a function of position on the virial sphere, and explore correlations between orbital properties and the spin of the host halo.

Our aim is to provide a precise and accurate measurement of the distribution of orbital properties of substructures at the time of merging, and to provide fits to this distribution so that it may be used in further studies. This distribution could, in principle, depend on many quantities, such as the masses of the merging halos, redshift, cosmological parameters etc. Furthermore, the six parameters describing each orbit (e.g. the position and velocity of the satellite at the time of merging, or any equivalent parameter set) may well be correlated with each other, such that we should really examine a six-dimensional phase-space distribution function. With the currently available N-body simulations we will limit ourselves to exploring a two-dimensional function, typically that of radial and tangential velocities (effectively assuming that infalling satellites are uniformly distributed on a sphere around the halo centre and that their tangential velocities have no preferred direction), although we will explore correlations between these quantities and the host halo. We note also that the situation could in principle be more complicated still. We are aiming to quantify $P(\mathbf{x})$, where \mathbf{x} are the orbital parameters and P is the distribution of these averaged over all merging events. However, after one merger with parameters \mathbf{x}_1 the relevant distribution function for the next merger may be different, $P(\mathbf{x}|\mathbf{x}_1)$. An example might be infall of halos along a filament. Knowing that one halo fell in from a particular direction, it becomes more likely that the next halo will fall in from a similar direction. We will explore one aspect of this possibility by measuring the distribution of angles between pairs of infalling satellites.

The remainder of this paper is arranged as follows. In §2 we describe our analysis technique while in §3 we present our results. We give our conclusions in §4.

¹ Since the orbital parameters are constantly changing for such orbits, the eccentricity and peri-centric distance no longer have the advantage of being constant along the orbit. The orbital velocities are more closely related to the quantities required by semi-analytic orbital models so we prefer to use them. The two pairs of orbital parameters (eccentricity+semi-major axis and radial+tangential velocity) are, of course, equivalent.

2 ANALYSIS

2.1 N-body Simulations

To measure satellite orbital parameters we make use of a large number of N-body simulations carried out by the VIRGO Consortium and which are publicly available (see Jenkins et al. 1998; Kauffmann et al. 1999.; Jenkins et al. 2001 for further details), together with one other simulation used for testing various aspects of our methodology. These span a range of cosmologies and redshifts. Details of the simulations used are given in Table 1. All of the outputs from these simulations are analysed, but in practise only those at redshifts $z \lesssim 2$ provide statistically useful measurements of orbital parameter distributions.

2.2 Group Finding

In order to find merging dark matter halos in the simulations we must first identify all dark matter halos. To locate dark matter halos in the N-body simulations we employ two standard group finders, the friends-of-friends (FOF; Davis et al. 1985) and spherical overdensity (SO; Lacey & Cole 1994) algorithms. We will compare results for halos found using these two techniques to test for any dependence on the group finding algorithm used.

Each algorithm has one tunable parameter, the linking length, r_{link} , for the FOF algorithm and the mean density contrast inside the sphere, $\bar{\Delta}$, for the SO algorithm. Both can be related to the mean density of dark matter halos (once a specific halo density profile has been chosen in the case of the FOF algorithm). We apply each algorithm twice, once assuming a mean overdensity for halos of $\bar{\Delta} = 18\pi^2 \approx 177.7$ (equivalent to $r_{\text{link}} = 0.20\bar{r}$, assuming an isothermal halo profile², where \bar{r} is the mean inter-particle spacing in the simulation), as expected from the spherical collapse model in a critical density cosmology (e.g. Peebles 1980), and once using the mean overdensity expected from the spherical collapse model for the specific cosmology and redshift in question (Lacey & Cole 1993; Eke, Cole & Frenk 1996). We will refer to these two alternatives as “fixed Δ ” and “variable Δ ” respectively, and will compare results from the two.

Once halos have been located by either algorithm we apply a procedure to remove unbound halos from the resulting catalogue. Our technique is described fully by Benson et al. (2001) and involves repeatedly removing the least bound particle from an unbound halo until the halo either becomes bound, or falls below the minimum mass required to be included in our catalogue.

² It is well known that cold dark matter halos are not well approximated by isothermal spheres. However, if we instead adopt an NFW density profile (Navarro, Frenk & White 1997) for our halos the appropriate value of r_{link} ranges between $0.22\bar{r}$ and $0.26\bar{r}$ for halos with concentrations in the range 5 to 15. As such, a somewhat larger value of r_{link} may be appropriate. Nevertheless, we will retain the convention of assuming isothermal halos here and resign a study of the most appropriate linking length to use to future work.

Table 1. The names, parameters and output redshifts of the N-body simulations used in our analysis. The first two columns give the name of the simulation set and the cosmological model respectively. Columns 3 lists the number of particles in each simulation, while columns 4 and 5 list the cosmological parameters Ω_0 and Λ_0 appropriate to each simulation. Column 6 specifies the length of the simulation cube, while column 7 specifies the mass of each particle in the simulation. Column 8 gives the softening length used in the simulation. Finally, column 9 lists the redshifts at which outputs from the simulation are available.

Simulation	Model	Particles	Ω_0	Λ_0	$L/h^{-1}\text{Mpc}$	$m_p/h^{-1}M_\odot$	$l_{\text{soft}}h^{-1}\text{kpc}$	Redshifts
GIF	ΛCDM	256^3	0.3	0.7	141.3	1.4×10^{10}	20	50, uniform in $\ln(a)$ from $z = 50$ to $z = 0$
GIF	OCDM	256^3	0.3	0.0	141.3	1.4×10^{10}	30	0.0, 0.1, 0.3, 0.5, 1.0, 1.5, 2.0, 3.0, 5.0
GIF	SCDM	256^3	1.0	0.0	84.5	1.0×10^{10}	36	0.0, 0.1, 0.3, 0.5, 1.0, 1.5, 2.0, 3.0, 5.0
GIF	τCDM	256^3	1.0	0.0	84.5	1.0×10^{10}	36	0.0, 0.1, 0.3, 0.5, 1.0, 1.5, 2.0, 3.0, 5.0
GIF-II	τCDM	256^3	1.0	0.0	84.5	1.0×10^{10}	36	0.0
Virgo	ΛCDM	256^3	0.3	0.7	239.5	6.86×10^{10}	25	0.0, 0.1, 0.3, 0.5, 1.0, 1.5, 2.0, 3.0, 5.0
Virgo	OCDM	256^3	0.3	0.0	239.5	6.85×10^{10}	30	0.0, 0.1, 0.3, 0.5, 1.0, 1.5, 2.0, 3.0, 5.0
Virgo	SCDM	256^3	1.0	0.0	239.5	2.27×10^{11}	36	0.0, 0.1, 0.3, 0.5, 1.0, 1.5, 2.0, 3.0, 5.0
Virgo	τCDM	256^3	1.0	0.0	239.5	2.27×10^{11}	36	0.0, 0.1, 0.3, 0.5, 1.0, 1.5, 2.0, 3.0, 5.0
ff VLS	ΛCDM	512^3	0.3	0.7	479.0	6.86×10^{10}	30	0.0, 0.5, 1.0, 2.0, 3.0, 5.0

2.3 Defining the Halo Centre

To measure orbital properties of infalling satellites we need to define a centre (both in position and velocity) for each halo in order to have a suitable origin for our coordinate system. The simplest option is to determine the centre of mass and the mass weighted mean velocity of the halo and take these as the origin. We call this ‘‘COM centring’’. Because of its simplicity we will examine results based upon this approach. However, while a simple centre of mass estimate of the halo centre is reasonable if halos are smooth, spherical systems, in reality it has many failings (particularly when applied to FOF halos). The FOF algorithm often links together halos that are about to merge by a low density ‘‘bridge’’ of particles. This will skew the centre of mass of the halo away from what perhaps should be considered the centre (e.g. the position corresponding to the centre of mass of the main component of the merging system). Because of this limitation we will adopt a second approach in which we define the centre of a halo as being the position of the particle with the lowest gravitational energy (counting only interactions with other particles in the halo). This will naturally pick out a particle in the densest region and, given two halos joined by a low-density bridge should pick out a particle in the more massive of the two halos. However, we cannot take the velocity of this particle as being representative of the velocity of the halo, since its motion will consist of the mean halo motion plus a component due to the halo’s internal velocity dispersion. Unfortunately, just as in position space, halos in velocity space can show bimodal distributions (as happens when a halo is linked to a nearby halo which is infalling). This can bias the mass weighted mean velocity estimate of the origin away from the ‘‘correct’’ value. To circumvent this problem we adopt a similar approach in velocity space as in position space. Namely, we estimate an ‘‘energy’’, ϵ , for each particle, i , using $\epsilon_i = \sum_{j \neq i} -1/|\mathbf{v}_i - \mathbf{v}_j|$, with the sum taken over all particles in the halo, and then locate the particle with the lowest energy. This should lie close to the true mean motion of the halo. We call this method ‘‘MBP centring’’.

It is worth noting that the velocity origin can differ significantly between the two definitions we adopt. Fig. 1 shows the centre of a particular halo from the $z = 0$ output of the GIF ΛCDM simulation in both position and velocity

space. Each frame has its origin on the most-bound particle, as marked by the dashed lines, while the dotted lines indicate the centre of mass or mass-weighted mean velocity. In this example, the centre of mass almost coincides with the most bound particle (somewhat fortuitously as nearby halos on either side, linked in by the FOF algorithm, are cancelling each other out). In velocity space however, we see that the velocity origin is shifted by over 500km/s from the more realistic velocity origin. This could seriously affect our estimates of orbital parameters.

2.4 Satellite Orbital Parameters

From our catalogue of dark matter halos in each simulation we search for pairs of halos which are about to merge. From here on, all velocities are measured in units of the virial circular velocity of the host halo, V_{vir} , and all radii in units of virial radius of the host halo, r_{vir} , as we expect these to be characteristic scales of the systems³. We search for halos within a distance from the host centre between $r = 1 \pm \Delta r$, and which have an inward directed velocity, \mathbf{v} (i.e. $\mathbf{r} \cdot \mathbf{v} < 0$ where \mathbf{r} is the vector from the centre of the host to the centre of the potential satellite halo). We choose $\Delta r = 0.2$. Note that we allow for the possibility of halos with $r < 1$ since the non-spherical shape of real halos can permit a halo to remain separate from the host even when $r < 1$. It should be noted that this radial selection biases us against finding mergers between halos of comparable mass (since in this case it is unlikely that the satellite will remain as an isolated halo once its centre is within $1 + \Delta r$). For present purposes this bias is unimportant, and so we retain the above criterion for simplicity. This bias could however, be easily circumvented by adopting a radial selection based upon the sum of the host and satellite virial radii instead. From the halos selected in this way, we compute the radial and tangential components

³ We convert the comoving coordinates of the N-body simulation to physical coordinates and add on the Hubble flow to the peculiar velocities taken from the N-body simulations. Halo virial radii and velocities are determined from their masses assuming the halo to have the mean density appropriate to a just-collapsed spherical top-hat overdensity.

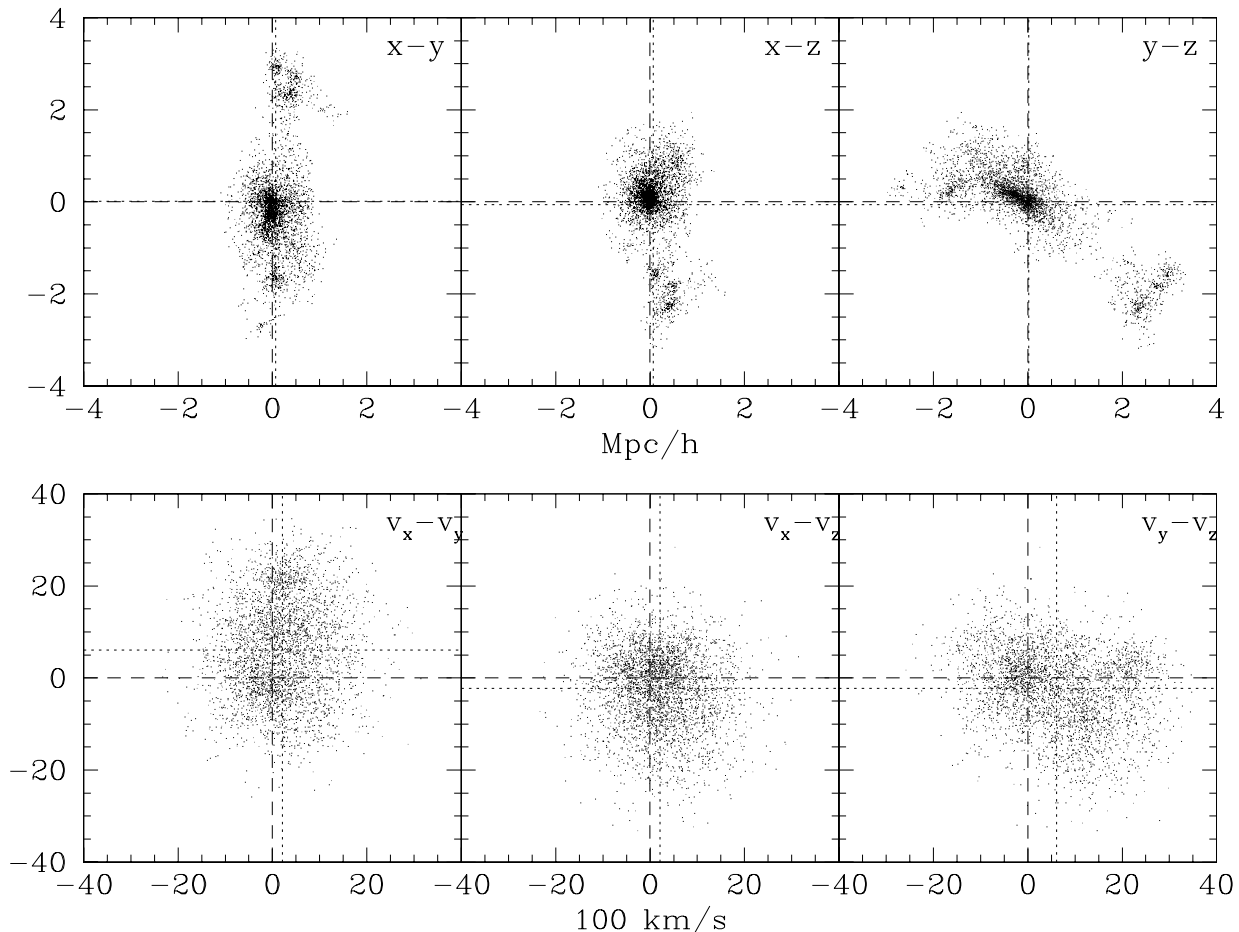


Figure 1. The results of using the COM and MBP algorithms to define the origin of the coordinate system in a dark matter halo identified in the $z = 0$ output of the GIF Λ CDM simulation. The upper row shows three projections of the spatial distribution of particles. The intersection of the dashed lines indicates the origin according to the MBP algorithm, while that of the dotted line indicates the origin according to the COM algorithm. The lower row shows projections of the same halo in velocity space. Dashed and dotted lines are as in the upper row.

of velocity. We also store the three dimensional position and angular momentum of the merging satellite.

Since we are interested in the orbital parameters of satellites as they cross the virial radius of a larger halo we correct our orbital parameters (which are measured at some radius close to, but not equal to, the virial radius). To do this we treat the two halos as point masses, and simply determine the point at which the satellite’s orbit first crosses the virial radius of the larger halo. We store the position, velocity and angular momentum of the satellite at this point. This approach is an approximation for two reasons. Firstly, as the host halo is not a point mass, the mass interior to the substructure’s orbit will change along that orbit. In practise this effect is quite small, leading to only a 5% error in the orbital velocities. (Note also that the density profile is not spherically symmetric, which will lead to further errors.) Secondly, we neglect the effects of dynamical friction on the orbital parameters. A simple estimate based upon Chandrasekhar’s methods indicates that this would lead to an error in our orbital velocities of around 10% for a substructure to host

mass ratio of 0.08 (which is typical of the systems found in our simulations), scaling approximately in proportion to this ratio. All of these problems could be largely overcome by solving the equations of motion for the substructure in a realistic host potential including a dynamical friction term. This will be the focus of future work.

Some fraction of substructures are found to be on unbound orbits. This presents no problem for our analysis, we can of course still measure the orbital parameters of such substructures, and so we retain these objects in our calculations. The fate of such substructures will be discussed below. Some substructures are found with $r < 1$ —already inside the virial radius by our definition. These substructures are propagated backwards along their orbit to find their orbital parameters at the time of crossing $r = 1$ (as with all orbits, no account is made for any mass loss which might have occurred from these halos, nor for the effects of dynamical friction). Finally, we find some halos whose orbits do not cross the virial radius of the host. Such halos are flagged

as being “bad” and are treated separately from other halos (see §3.1.2).

We must also account for the fact that our selection of halos with $1 - \Delta r < r < 1 + \Delta r$ leads to a bias against finding radial orbits as they will spend less time in this region than more circular orbits. To correct for this we simply determine, from the measured orbital parameters of the satellite, the time, δt , it takes to traverse the region $r = 1 + \Delta r$ to r_{\min} . Here r_{\min} is the minimum radius at which the satellite halo would have been identified by the group finder. When constructing distributions of orbital parameters we then weight by $\Delta t / \delta t$ where Δt is the cosmic time between the current N-body simulation output and the previous one (or $t = 0$ in the case of the highest redshift output).

The determination of r_{\min} depends on the group finder used. With the SO group finder it is relatively easy to determine r_{\min} . Under the SO algorithm each halo is assigned a radius (the radius containing a mean overdensity of some specified value). Once all halos have been found any halo whose centre lies within the radius, r_{SO} , of a larger halo is merged with that larger halo and removed from the list of individual halos. (Note that the radius of the larger halo is not changed by this merging.) Thus, r_{\min} is simply r_{SO} , or $1 - \Delta r$, whichever is larger.

For the FOF group finder things are a little more complicated as the halos found are not spherical. The satellite halo would no longer have been found as an isolated object by the group finding algorithm once any one of its particles came within a distance r_{link} of a particle in the larger halo. We therefore search for the first point along the orbit of the satellite at which any one of its particles comes within r_{link} of a particle in the larger halo. We define r_{\min} to be the orbital radius at this point, or $1 - \Delta r$, whichever is larger. The advantage of this approach is that it works even for the non-spherical halos found by the FOF algorithm. Its disadvantage is that it treats the orbit as that of two point masses and also ignores any internal evolution of the satellite or host halos during the time it takes the satellite to move along its orbit. This latter is not a problem providing the two halos are in internal equilibrium and not rotating since then, although the individual particles in the halos move, their distribution at any time provides a fair sample of the mass distribution of the halo at any later time. Of course, in reality the halos will not be in equilibrium (although we expect them to be close to it). In particular, the FOF algorithm is known to make “dumbbell-shaped” halos by linking together two halos by a low density bridge. These are certainly not equilibrium systems in the sense used here. They are also those in which the two-body orbit approximation is likely to be worst. We consider this to be a limitation of the FOF algorithm, and do not explore more complicated ways of dealing with this problem here.

It should be noted that, with our method for locating merging halos, some host halos may be experiencing mergers with multiple substructures at any given time. In fact, we find that about 25% of all of our merger events at $z = 0$ involve two or more substructures accreting onto the same host halo. For the largest clusters we find up to around twenty ongoing mergers in some cases. We find very few mergers with low mass ratios (e.g. less than 4:1). As such, the inclusion or not of hosts currently undergoing major mergers does not affect our results significantly.

3 RESULTS

We examine the orbital parameter distributions for each individual output of each simulation. We will also combine results together where possible to improve the statistical precision. All results will make use of the FOF halo finding algorithm, MBP halo centring and the variable Δ method for setting $r_{\text{link}}/\bar{\Delta}$ unless otherwise stated.

Figure 2 shows an example of the distribution of orbital parameters that we measure. The distribution of radial and tangential velocities (upper left and right-hand panels respectively) have quite simple, and perhaps unsurprising, forms, being peaked at $V \sim 1$ with a dispersion of order unity. The infall angle, defined as the (negative of the) angle between the infalling substructure’s radius and velocity vectors (i.e. $\phi = -\cos^{-1} \mathbf{r} \cdot \mathbf{v} / (|\mathbf{r}| |\mathbf{v}|)$), is shown in the lower-left hand panel. This distribution will be investigated further in §3.3. Finally, the lower right-hand panel shows the two-dimensional distribution of radial and tangential orbital velocities. It is clear that there is a significant correlation between these two parameters. Another interesting feature of this distribution is that a significant fraction of orbits drawn from this distribution are initially unbound. The energy of orbits, in our units, is given by

$$E = -1 + \frac{1}{2f_2} \left(V_r^2 + \frac{(2 - f_2)^2}{f_2^2} V_\theta^2 \right), \quad (1)$$

where $f_2 = 1 + M_2/M_1$. Note that $f_2 \equiv M_2/\mu$ where $\mu = M_1 M_2 / (M_1 + M_2)$ is the usual reduced mass. The dotted line in Fig. 2 shows the line $E = 0$ for the case $f_2 = 1$ (i.e. $M_1 \ll M_2$). Points to the upper right of this line correspond to unbound orbits. For the particular distribution shown about 18% of all orbits are unbound. We choose to retain these orbits for two reasons:

- (i) When using the measured distribution to select initial orbits for satellites, unbound orbits can easily be discarded if desired.
- (ii) Due to the effects of dynamical friction, an orbit that starts out unbound will not necessarily stay that way.

To examine the importance of this second point we employ the semi-analytic model of Benson et al. (2004) which follows the cosmological growth of dark matter halos (and their associated galaxies) including a detailed treatment of the orbital evolution of satellite halos. In Benson et al. (2004) the initial orbits of merging satellites were determined by setting the energy of each orbit equal to that of a circular orbit at half the virial radius and choosing a circularity (i.e. the angular momentum of the satellite in units of that of a circular orbit with the same energy) from a uniform distribution between 0.1 and 1.0. These choices were motivated by the results of Ghigna et al. (1998). Here, we instead use the measured distribution of orbital velocities, including unbound orbits, to set the initial velocity of satellites, and choose their initial position at random on a sphere with radius equal to the virial radius of their host. From this cosmologically representative sample of halos and orbits, we identify those which start out unbound. Of these, some fraction will lose sufficient energy through dynamical friction that they become bound by the endpoint of their evolution (i.e. by $z = 0$) while others will fail to do so and will instead leave their host halo with positive energy. We

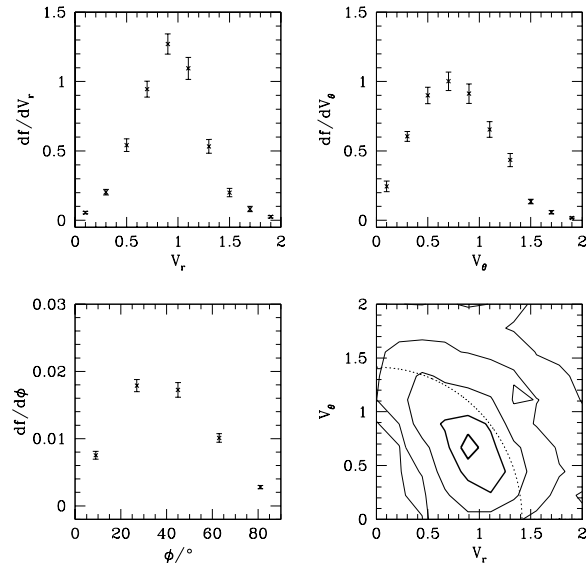


Figure 2. Distributions of orbital parameters measured in the VLS plus VIRGO Λ CDM $z = 0$ output. Upper left and right-hand panels show distributions of radial and tangential velocities respectively. The lower left-hand panel shows the distribution of infall angles, while the lower right-hand panel shows the two-dimensional distribution of radial and tangential velocities. Contours are drawn at $d^2f/dV_r dV_\theta = 0.01, 0.1, 0.5, 1.0$ and 1.4 from lightest to heaviest lines. The division between bound and unbound orbits in this panel is shown by the dotted line.

find that approximately 2% of all initially unbound orbits (equivalent to 0.3% of all orbits) fail to become bound and so escape their halo. As such, these “lost” satellites are only a small fraction of the total.

Our results are in good agreement with previous work. Figure 3 shows a comparison of the distribution of tangential velocities with that found by Vitvitska et al. (2002; our V_θ is equivalent to their L/L_{vir}). Although the two distributions differ as judged by a χ^2 test, the discrepancy is due to two points and plausibly reflects our ignorance of the true errors and the differences in the simulations (e.g. softening, method of force calculation etc.) used in this work and that of Vitvitska et al. (2002).

3.1 Tests of the Distributions

Firstly, we examine which, if any of our measured distributions are consistent with each other. This will allow us to determine which distributions we can realistically average together in order to improve the statistical precision of our measurements.

3.1.1 Calibration of χ^2

We adopt a simple χ^2 test to determine if two of our measured two-dimensional velocity distributions are consistent with each other. It should be noted that the errors which we determine for our distributions are likely to be an underestimate—they account for the finite number of mergers in each bin, but ignore such contributions as errors in

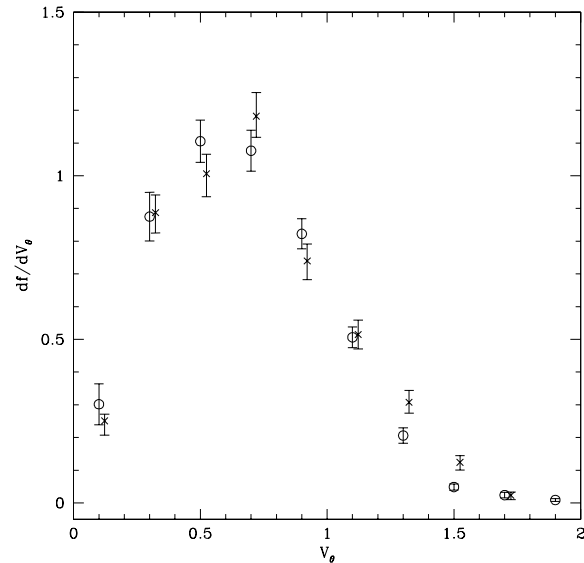


Figure 3. The distribution of tangential velocities for orbits. Circles show results for the VLS plus VIRGO Λ CDM simulations $z = 0$ output from this work, while crosses (offset horizontally slightly for clarity) show the results of Vitvitska et al. (2002).

our determinations of orbital velocities etc. Given this, and the fact that our errors may not be normally distributed, we would ideally like a calibration of the χ^2 test. To achieve this we compare distributions from our GIF and GIF-II τ CDM $z = 0$ simulations. Comparing both the FOF and SO results, with halo centres defined using both centre of mass and most bound algorithms we find values of χ^2 per degree of freedom which scatter around unity, with a mean of 1.05. Although we would ideally like many more independent simulations to test our errors this gives us confidence that the errors are a good approximation to the true uncertainty on each data point.

3.1.2 Distribution With and Without “Bad” Orbits

A small fraction of the orbits that we find are flagged as being “bad” in the sense that they do not pass through one or both of the radial limits which we use for computing the weight to assign to each orbit. This may represent cases in which a halo formed within the outer radial limit (and so never passed through it), or, more likely, a limitation of the simple, two-body orbit neglecting dynamical friction that we use to approximate the motion of the halos. The best guess at a suitable weight for these orbits is to use their instantaneous radial velocity to determine the time taken to cross between the two radial limits. However, we find that the resulting distributions of orbital parameters for bad orbits differ significantly (as judged by the χ^2 test) from those of good orbits. Therefore, we adopt the approach of excising all bad orbits from our distributions. Ideally, we should deal with these better by solving for the orbit correctly (i.e. including extended masses and dynamical friction) to see if they really do merge and thereby assigning a realistic weight.

3.1.3 Number of particles per halo

Our halo finding algorithms retain only halos consisting of ten particles or more. To test whether particle number has any effect on the measured distribution of orbit parameters we compare measurements of the orbit distribution in the VLS and VIRGO simulations with the equivalent GIF simulations, keeping halos with 10 or more particles in the VIRGO and VLS simulations and adopting an equivalent mass cut in the GIF simulations (49 or more particles per halo in the Λ CDM and OCDM simulations and 227 or more particles in the SCDM and τ CDM simulations), such that the minimum mass of halos in each simulation is the same (this avoids any consequences of possible mass-dependent trends in the orbits).

We find no evidence of any significant difference between the velocity distributions constructed from halos with 10 or more particles and those with 5–20 times more particles from the GIF simulations. The measured values of χ^2 per degree of freedom are scattered around unity and are consistent with being drawn from a χ^2 distribution (as judged by a K-S test).

While we would ideally like more extensive tests of the effects of particle number⁴ we are confident that by using halos containing ten or more particles we are obtaining an accurate measure of the distributions.

3.1.4 Radial search limits

We also wish to test whether our imposed limits on the radial separation of halos affects the distributions. To do this we use the independent GIF and GIF-II τ CDM $z = 0$ outputs. Velocity distributions are constructed from both simulation outputs using radial search limits between $\Delta r = 0.01$ and $\Delta r = 0.20$ in steps of 0.01. We then compute the χ^2 statistic comparing the GIF simulation with $\Delta r = 0.20$ to the GIF-II simulations with $\Delta r < 0.2$, and vice versa. We find that the χ^2 values stay reasonably constant as the radial search limit is decreased, and certainly show no signs of becoming significantly larger than unity. As such, we conclude that the $\Delta r = 0.2$ search limit is sufficiently small to allow an accurate determination of the velocity distributions.

3.2 Trends

Having established that the techniques employed in this paper are able to accurately determine the distribution of orbital velocities for infalling satellites we proceed to search for any dependence of those distributions on the masses of the halos, redshift and cosmology. When testing for such dependence we adopt the approach of varying only one variable at a time, with the hope of isolating the cause of any trend we discover. While this is crucial to developing an understanding of the trends it significantly limits the number of comparisons that we can make.

⁴ Ideally we would like a set of simulations identical in all respects apart from the number of particles used. This would permit direct comparisons of the orbital parameters of individual merging events to be made.

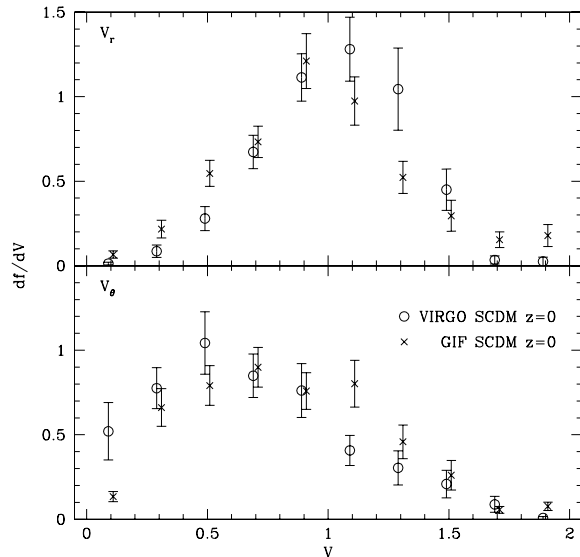


Figure 4. Distributions of radial (upper panel) and tangential (lower panel) velocities for the GIF and VIRGO SCDM $z = 0$ outputs.

3.2.1 Mass Dependence

Since our distributions are constructed by combining the orbits of all the halos, irrespective of mass, in a given simulation output it is crucial that we first test for the presence of any trends with mass. To test for mass-dependent trends we compare the GIF simulations with the VIRGO and VLS simulations. These have identical cosmological parameters, and we use halos with 10 or more particles in each simulation. The only difference then is the particle mass and the corresponding mass function of dark matter halos.

We find evidence for mass-dependence in the distributions of orbital parameters. Figure 4 shows distributions of radial and tangential velocities for GIF and VIRGO SCDM models at $z = 0$. There is a clear difference between the two, with the VIRGO simulation showing larger radial and lower tangential velocities on average. Unfortunately, our samples of mergers remain too small to provide an accurate determination of the nature of the mass dependent trends.

3.2.2 Redshift and cosmology

We next explore trends with redshift by comparing the results of outputs from the same simulation at different epochs. Specifically we compute χ^2 for pairs of outputs which differ by at least 50% in $1 + z$ to ensure that the samples are independent. We find strong evidence for differences between these samples. However, as the mass function of dark matter halos is a function of redshift, we cannot disentangle any redshift-dependent trend from the known mass-dependent trends. The current simulations do not possess enough halos to allow us to select a sub-sample of mergers by mass at each redshift in order to eliminate this problem. We also find significant differences between models with different cosmological parameters, but again cannot disentangle any possible mass-dependent trends. To fully address

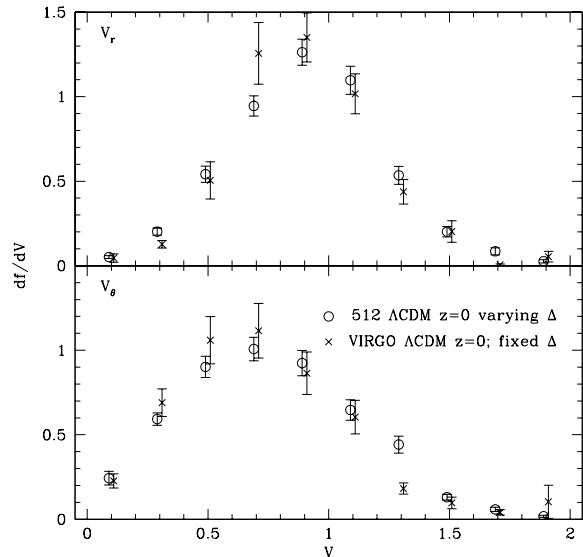


Figure 5. Distributions of radial (upper panel) and tangential (lower panel) velocities for the VIRGO OCDM and SCDM $z = 0.10$ outputs.

these issues will require a set of custom N-body simulations designed to allow us to explore changes in the orbital parameter distributions in a controlled manner. (For example, the current simulations have a variety of softening lengths, which may affect our results. A dedicated set of N-body simulations could explore the effects of this parameter on the distributions recovered.)

3.2.3 Group Finding Algorithm

We test for possible dependence on the group finding algorithm by comparing distributions of orbital velocities from the VLS Λ CDM simulation with halos found using the FOF group finder, to those from the VIRGO Λ CDM simulation with halos found using the SO group finder. We find no evidence for any systematic difference between the distributions based upon these two group finders, and so use the FOF algorithm throughout the remainder of this work.

3.2.4 Linking Length

We test for possible dependence on the linking length by comparing distributions of orbital velocities from the VLS Λ CDM simulation with halos found using the fixed (varying) Δ , to those from the VIRGO Λ CDM simulation with halos found using the varying (fixed) Δ . The distributions are found to be formally inconsistent with one another. Figure 5 shows a comparison. With the current statistical precision it is difficult to determine the exact nature of the difference between fixed and varying Δ distributions. We will thus not explore this further, and will continue to use the varying Δ method.

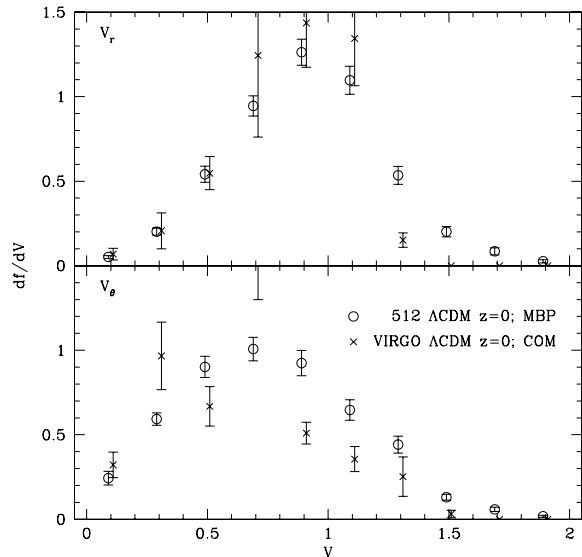


Figure 6. Distributions of radial (upper panel) and tangential (lower panel) velocities for the VLS and VIRGO Λ CDM $z = 0$ outputs.

3.2.5 Halo Centring Algorithm

We test for possible dependence on the halo centring algorithm by comparing distributions of orbital velocities from the VLS and VIRGO Λ CDM simulations with halos found using each algorithm (COM and MBP). The distributions are again found to be formally inconsistent with one another. In Figure 6 we show a comparison for the $z = 0$ simulation outputs. The differences between the two distributions are clearly visible. We find that the COM algorithm typically produces distributions of radial and tangential velocities which peak at lower values than the MBP algorithm. As we demonstrated in Fig. 1, the COM algorithm can easily find an unrealistic origin in both position and velocity space. Figure 6 shows that this problem can significantly affect the resulting distribution of orbital parameters. We prefer to use the more robust MBP algorithm, and do so throughout the remainder of this paper.

3.3 Fitting Functions

The results presented in this work are potentially of great value to any study involving the evolution of the substructure population of cold dark matter halos. To facilitate their use in this way we provide a simple fitting function which describes the two-dimensional distribution of orbital velocities. Through simple variable transformations this function also describes the distributions of substructure energies, angular momenta, eccentricities etc.

We find that our measured two-dimensional distributions of orbital velocities can be reasonably well fit with the following fitting function:

$$f(v_r, v_\theta) = a_1 v_\theta \exp \left[-a_2 (v_\theta - a_9)^2 - b_1 (v_\theta) \{v_r - b_2 (v_\theta)\}^2 \right], \quad (2)$$

where

$$b_1(v_\theta) = a_3 \exp \left[-a_4 (v_\theta - a_5)^2 \right], \quad (3)$$

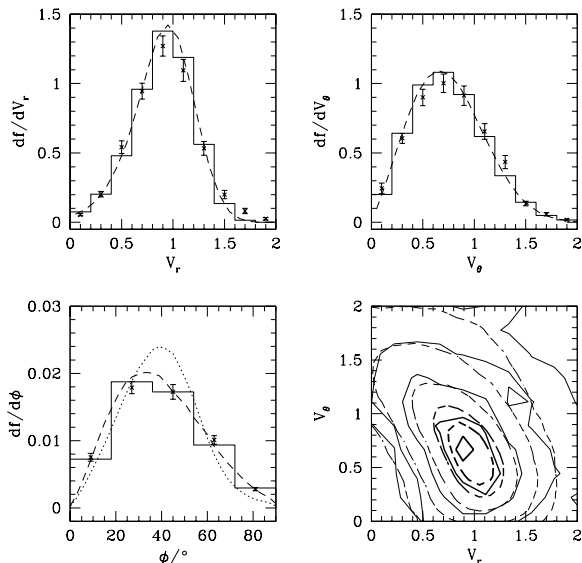


Figure 7. Distributions of orbital parameters measured in the VLS plus VIRGO Λ CDM $z = 0$ outputs are shown by crosses. Upper left and right-hand panels show distributions of radial and tangential velocities respectively. The lower left-hand panel shows the distribution of infall angles, while the lower right-hand panel shows the two-dimensional distribution of radial and tangential velocities (solid contours). Dashed lines show the fitting function, while histograms show this function averaged over the same bins as used to measure the distributions. The dotted line in the lower left-hand panel indicates the distribution of infall angles that would occur if correlations between V_r and V_θ were ignored.

$$b_2(v_\theta) = a_6 \exp[-a_7(v_\theta - a_8)^2]. \quad (4)$$

$$(5)$$

Note that this has a form similar to a two-dimensional Maxwell-Boltzmann distribution for the tangential velocity and a Gaussian for the radial velocity, as might be expected from the results of Vitvitska et al. (2002). However, the mean and dispersion of the radial velocity distribution are a function of the tangential velocity, as is necessary to account for the correlation between these two velocities found in our distributions.

We have fit this function to distributions of orbits taken from the combined VLS and VIRGO Λ CDM simulations (the VLS simulation is the only one which provides sufficient signal to noise to make fitting worthwhile). Figures 7 through 9 show distributions of orbital velocities together with the fitting function, while Table 2 lists the parameter values used in the fits.

3.4 Other quantities

Other quantities which characterise the satellite orbits are easily derived from the two velocities V_r and V_θ . For convenience, we list below expressions for several other orbital parameters in terms of these velocities.

Specific energy:

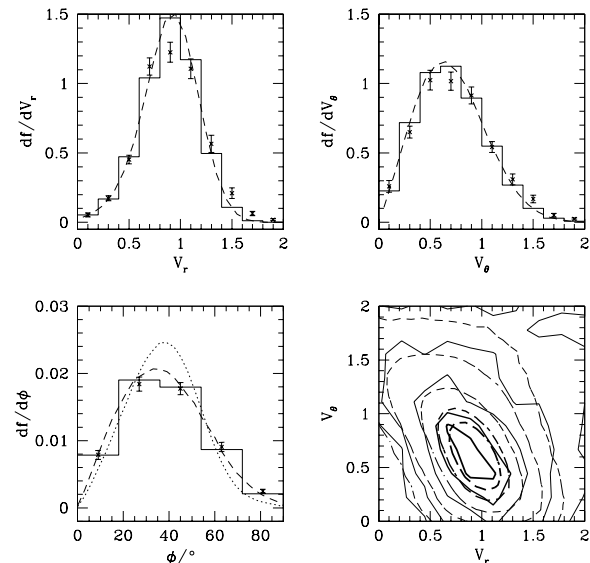


Figure 8. As Figure 7 but for $z = 0.5$.

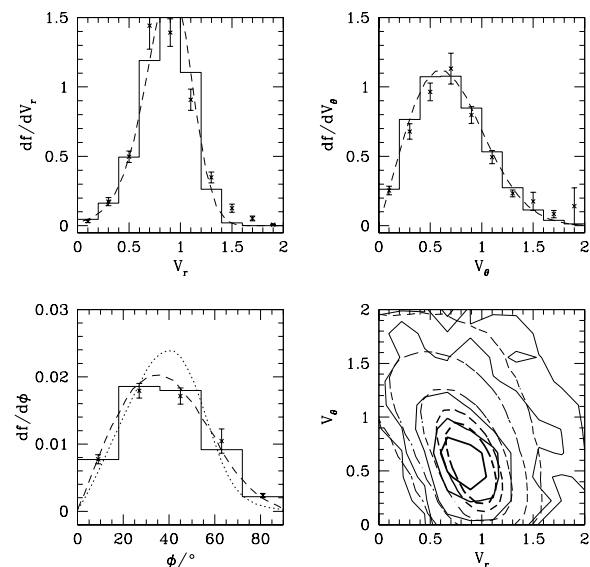


Figure 9. As Figure 7 but for $z = 1.0$.

$$E = -1 + \frac{1}{2f_2} \left(V_r^2 + \frac{(2 - f_2)^2}{f_2^2} V_\theta^2 \right), \quad (6)$$

Specific angular momentum:

$$J = V_\theta \quad (7)$$

Eccentricity:

$$e = \frac{V_\theta^2}{f_2} \sqrt{\left(1 - \frac{f_2}{V_\theta^2}\right)^2 + \left(\frac{V_r}{V_\theta}\right)^2} \quad (8)$$

Circularity:

$$\epsilon = V_\theta \sqrt{\frac{2f_2 - V_r^2 - V_\theta^2}{2f_2 - 1}} \quad (9)$$

Table 2. Parameters of the fitting function given in eqn. (2). Each column lists parameters which best fit distribution of orbital parameters in the combined VLS and VIRGO Λ CDM simulations at the specified redshift.

Parameter	Redshift		
	0.0	0.5	1.0
a_1	3.90	4.46	6.38
a_2	2.49	2.98	2.30
a_3	10.2	11.0	18.8
a_4	0.684	1.11	0.506
a_5	0.354	0.494	-0.0934
a_6	1.08	1.16	1.05
a_7	0.510	0.261	0.267
a_8	0.206	-0.279	-0.154
a_9	0.315	0.331	0.157

Semi-major axis:

$$a = \frac{f_2}{2f_2 - V_r^2 - V_\theta^2} \quad (10)$$

Pericentric distance:

$$r_{\text{peri}} = \left[\frac{f_2}{V_\theta^2} + \sqrt{\left(1 - \frac{f_2}{V_\theta^2}\right)^2 + \left(\frac{V_r}{V_t}\right)^2} \right]^{-1} \quad (11)$$

Apocentric distance:

$$r_{\text{apo}} = \left[\frac{f_2}{V_\theta^2} - \sqrt{\left(1 - \frac{f_2}{V_\theta^2}\right)^2 + \left(\frac{V_r}{V_t}\right)^2} \right]^{-1} \quad (12)$$

3.4.1 Eccentricity and semi-major axis

We have presented results for radial and tangential velocities, but of course can just as easily examine invariant parameters of the orbits, such as eccentricity and semi-major axis. Figure 10 shows distributions of these two parameters from the VLS Λ CDM $z = 0$ output, together with the distributions implied by our fitting function. Our distribution of eccentricities is qualitatively, but not quantitatively, in agreement with that presented in the first version of the preprint (i.e. `astro-ph/0309611` version 1, hereafter Khochfar & Burkert (2004) v.1) by Khochfar & Burkert (2004), with most orbits being close to parabolic ($e = 1$). We find that almost half of all orbits have $e = 1 \pm 0.1$, a somewhat smaller fraction than the 70% given by Khochfar & Burkert (2004) v.1.

In fact, as we show in Fig. 11 our results are significantly different from those of Khochfar & Burkert (2004) v.1. Comparing results from this work with those of Khochfar & Burkert (2004) v.1 we find that our results, though peaked around $e = 1$, are more broadly distributed. Khochfar & Burkert (2004) use a different approach to finding merging halos than we do⁵ and this could potentially in-

⁵ Briefly, they locate the progenitors of a given halo at a slightly earlier redshift. They then measure the orbital properties of these progenitors, providing they are separated by more than the sum of their virial radii. To ensure that the apparently merging halos

fluence the results obtained. We have implemented Khochfar & Burkert’s (2004) methods on the GIF Λ CDM simulations to test for any systematic effects caused by the difference in methods. We have checked that our implementation produces eccentricities identical to theirs (Khochfar, private communication). Khochfar & Burkert (2004) v.1 did not add on the Hubble flow velocity to the motions of halos (Khochfar, private communication). Using the Khochfar & Burkert (2004) methods we obtained the distributions shown by filled triangles and open squares in Fig. 11. (Filled triangles have no Hubble flow added to halo motions, while open squares do have the Hubble flow added.) We find that we are able to reproduce the results of Khochfar & Burkert when using only halo peculiar velocities in our calculations, and are able to reproduce our own results when the Hubble flow is included.

As a second check, we have taken the distribution of orbital circularities found by Tormen (1997), who used techniques similar to Khochfar & Burkert (2004), and converted these into eccentricities using eqns. (8) and (9) (assuming $f_2 = 1$). Correcting for the fact that orbits with $e > 1$ are not included in the distribution of Tormen (1997) we find an eccentricity distribution as shown by the crosses in Fig. 11.

We conclude that these two different approaches to determining distributions of halo orbital parameters produce consistent results, providing they attempt to measure the same quantities. The differences between the distributions of eccentricities reported here and by Khochfar & Burkert (2004) v.1 can be traced to the choice of whether to include the Hubble flow in particle velocities (as we did), or to use peculiar velocities, as did Khochfar & Burkert (2004) v.1⁶.

3.4.2 Correlations between pairs of infalls

We can test for correlations between the infall directions of pairs of satellites merging into the same halo. Figure 12 shows the distribution of angles ϕ between the radius vectors of pairs of satellites merging into the same host halo.⁷ Note

are not merely undergoing an unbound “fly-by” they also check that the centres of the halos have not moved further apart by a later redshift.

⁶ As a result of discussions regarding these differences, Khochfar & Burkert have revised their calculations to include the Hubble flow (see the published Khochfar & Burkert 2004 or version 2 of the preprint). Their results are then in good agreement with those found in this work, as shown by the stars in Fig. 11.

⁷ In this and subsequent figures exploring angles between pairs of satellites or satellites and the host halo spin we do not include our usual weights when constructing the distributions. Our weights reflect the fact that, due to the snapshot sampling provided by the N-body simulations) we do not see all mergers, but only those which occur within a short time after the snapshot. When constructing velocity (or eccentricity, semi-major axis etc.) distributions, the weighting used corrects for the unobserved population of mergers. To make the same correction when considering the infall angles here we must supplement the weight with an assumption about the angular distribution of the unobserved mergers. We make the simple assumption that the unobserved mergers have the same angular distribution as those which we do observe. As such, the resulting angular distribution is found from the observed mergers without any weights. Note that this

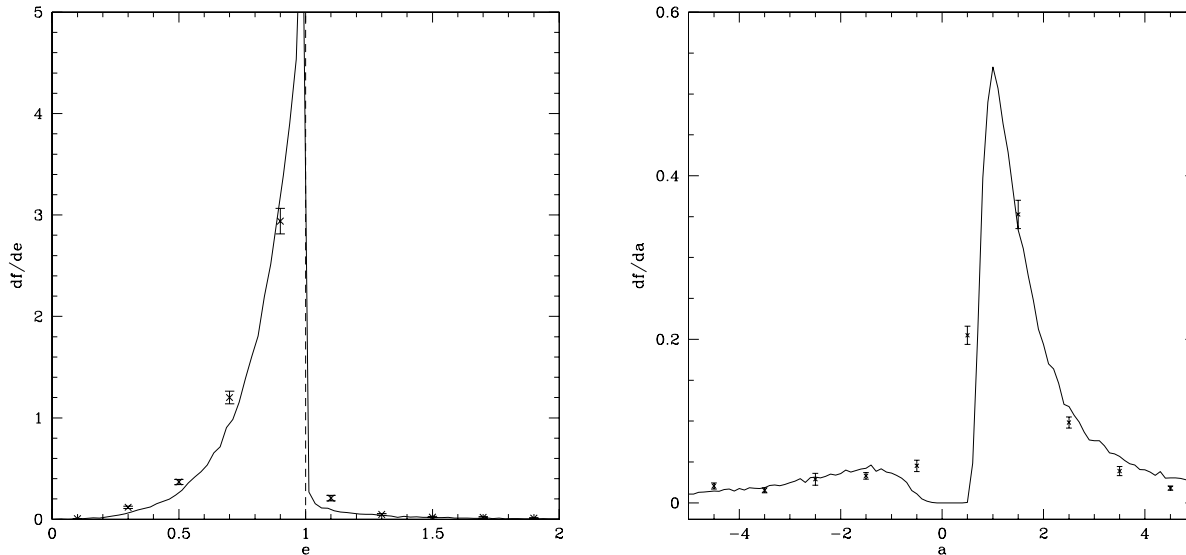


Figure 10. Distributions of eccentricity (left-hand panel) and semi-major axis (right-hand panel) for the VLS plus VIRGO Λ CDM $z = 0$ outputs are shown by the crosses with errorbars. The solid lines indicate the distribution resulting from the fitting formula of eqn. 2. The vertical dashed line the left-hand panel indicates parabolic orbits, and so the division between bound ($e < 1$) and unbound ($e > 1$) orbits. In the right hand panel, negative values of a correspond to unbound orbits. In this case the semi-major axis of the hyperbolic orbit is $|a|$.

that we have summed the results from all simulation outputs to obtain this distribution. This is permissible as our aim here is to search for any deviation from uncorrelated infall directions. As such, it does not matter if the different outputs are correlated in different ways—we would still see a difference from the null hypothesis of no correlations. The distribution appears to differ significantly from that expected if there were no correlations between infall directions. This correlation between infall directions is qualitatively as expected if mergers tend to occur along filaments, i.e. there is an enhancement in the number of mergers at small angles, $\zeta \lesssim 30^\circ$, with a corresponding suppression of mergers with angles around 90° .

3.4.3 Spin alignments

Finally, we can examine correlations between the infall direction and velocity of satellites and the spin angular momentum vector of the host halo. Figure 13 shows the resulting distributions. We find marginal evidence for deviations from a uniform distribution on the sphere. In particular, there is a suggestion that merging satellites have a tendency to have velocities normal to the spin axis of their host halo.

To assess the validity of these results will require a better calibration of our errors. For example, the direction of the spin vector may be poorly determined for low mass halos, a contribution to the errors that we do not take into account. (Although this effect should presumably weaken any correlations, implying that the true correlations are stronger than those we measure.)

assumption may be incorrect—for example, if the angular distribution correlates with infall velocity—but is at least simple.

4 DISCUSSION

We have described methods for determining the orbital parameters of dark matter halos at the point of merging with a larger system. Previous studies of the orbital properties of merging halos have typically considered the orbits after merging with the host halo, in which case the orbits will have changed due to dynamical friction. Other studies (Tormen 1997; Khochfar & Burkert 2004) used techniques which are restricted to simulations with closely spaced outputs if they are to be accurate. Furthermore, we have analysed a substantially larger number of orbits than has been previously possible to obtain improved statistical precision. This allows us to characterise in detail the two-dimensional distribution of infall velocities.

Our analysis pays particular attention to carefully identifying halos and their centres. We find that it is important to accurately identify the centre of the halo in both position and velocity space, and adopt a similar minimum “energy” definition for both of these. We have demonstrated that our results are unbiased by effects of particle number or radial search limit. In this work, we have focused on the two-dimensional distribution of radial and tangential velocities which we show has a relatively simple form. A fitting formula that describes this distribution is presented and should prove immensely valuable in future studies of satellite orbits.

Our methods could be improved upon in several ways. A set of simulations run with measurements of orbital parameters in mind would allow a better determination of the accuracy of our error estimates. More and larger simulations would also improve the statistical accuracy of our measurements and permit us to quantify the trends with, for example, mass that are apparent in the distributions. Finally, a more detailed treatment of the evolution of the satellite

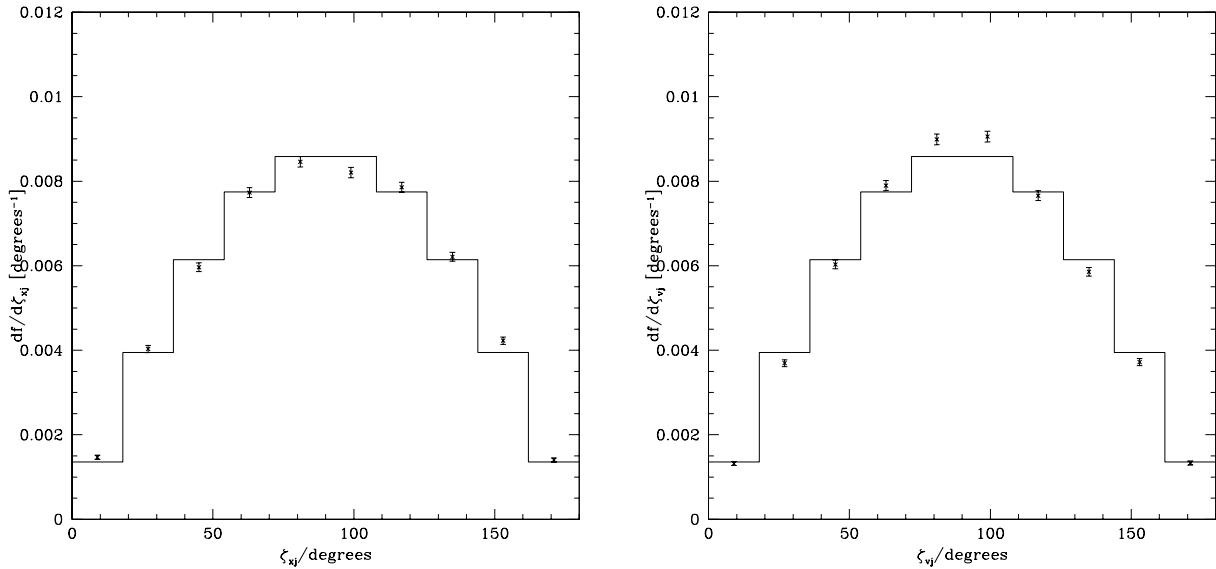


Figure 13. The distribution of angles between the infall direction (left-hand panel) and infall velocity (right-hand panel) of satellites and the angular momentum of the host halo. Points show results measured by summing merger events from all simulation outputs while histograms show the expectation when no correlations are present.

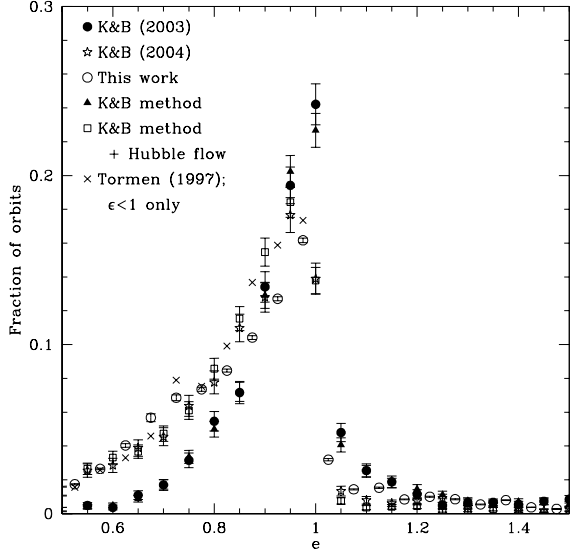


Figure 11. The distribution of orbital eccentricities. The quantity shown is the fraction of orbits in each eccentricity bin (i.e. following the format of Figure 1 of Khochfar & Burkert 2004). Filled circles indicate the results of Khochfar & Burkert (2004) v.1, while crosses show the results of Tormen (1997). Open circles are results from this work combining all redshifts from the GIF Λ CDM simulation using the MBP halo centring algorithm. Filled triangles show our implementation of Khochfar & Burkert’s (2004) methods when no Hubble flow is added to the velocities of particles in the N-body simulations, while open squares show the same with the Hubble flow added. Stars indicate the results of Khochfar & Burkert (2004) which represent the same calculation as Khochfar & Burkert (2004) v.1 revised to include the Hubble flow.

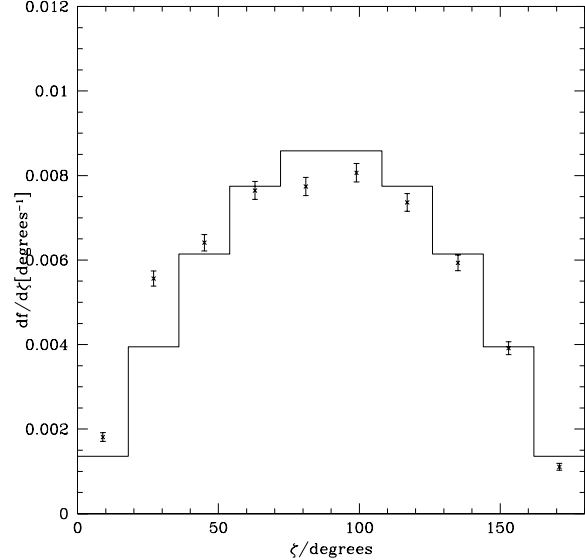


Figure 12. The distribution of angles between the infall directions of pairs of satellites merging onto the same host halo. Points show the distribution measured by summing results from all simulation outputs while the histogram indicates the expectation for uncorrelated infall directions.

orbits (including the effects of an extended, non-spherical host halo and dynamical friction) would remove sources of systematic error in our measurements. All of these factors will be the subject of a future paper.

We have presented evidence for the presence of trends with mass (and, perhaps, with redshift and cosmological parameters) in this distribution, although we are currently unable to accurately characterize these trends. Larger samples

of N-body halo mergers will allow us to both characterise these mass trends and to select sub-samples with a narrow range in mass to permit trends with redshift and cosmological parameters to be examined.

We have also explored the distribution of eccentricities and semi-major axes. We find that the eccentricity distribution is peaked around parabolic orbits ($e = 1$). This is qualitatively in agreement with the work of Khochfar & Burkert (2004) v.1. However, we find quantitative disagreements with their distribution of eccentricities. This disagreement has been traced to the fact that the Hubble flow was included in our calculations, while it was not included in those of Khochfar & Burkert (2004) v.1. Once Hubble flow is included, as in the final version of Khochfar & Burkert (2004), the results of the two studies are in excellent agreement. Our distributions of eccentricities and tangential velocities are also in good agreement with those from Tormen (1997) and Vitvitska et al. (2002) respectively.

Finally, we searched for correlations between the infall directions of pairs of satellites and between the infall positions and velocities of satellites and the angular momentum of their host halo. We find evidence that satellites infalling onto a given host tend to arrive from similar directions, compatible with the hypothesis that (at least some) infall occurs along filaments. We find marginal evidence that infall directions and direction of motion are aligned with the spin-axis of the host halo, although a more thorough study would be required to both confirm and interpret this possible correlation.

The evolution of sub-structures in cold dark matter halos is currently a topic of great interest. The tools provided in this work should prove of great value in further such studies while the techniques described should permit more accurate estimates of orbital parameter distributions (including dependences on halo mass, spin, redshift, cosmology etc.) to be constructed.

ACKNOWLEDGEMENTS

AJB acknowledges valuable discussions with Carlos Frenk, Joel Primack and T. J. Cox and thanks Sadegh Khochfar for providing data for Figure 11 in electronic form and for extensive discussions regarding eccentricity distributions. AJB also acknowledges support from a Royal Society University Research Fellowship. The simulations in this paper were carried out by the Virgo Supercomputing Consortium using computers based at Computing Centre of the Max-Planck Society in Garching and at the Edinburgh Parallel Computing Centre. The data are publicly available at www.mpa-garching.mpg.de/NumCos.

REFERENCES

- Abadi M. G., Bower R. G., Navarro J. F., 2000, MNRAS, 314, 759
- Benson A. J., Frenk C. S., Baugh C. M., Cole S., Lacey C. G., 2001, MNRAS, 327, 1041
- Benson A. J., Lacey C. G., Baugh C. M., Cole S., Frenk C. S., 2002, MNRAS, 333, 156
- Benson A. J., Lacey C. G., Frenk C. S., Baugh C. M., Cole S., 2004, MNRAS, 351, 1215
- Chiba M., 2002, ApJ, 565, 17
- Dalal N., Kochanek C. S., 2002, ApJ, 572, 25
- Davis M., Efstathiou G., Frenk C. S., White S. D. M., 1985, ApJ, 293, 371
- Diemand J., Moore B., Stadel J., 2004, MNRAS in press (astro-ph/0402160)
- Eke V. R., Cole S., Frenk C. S., 1996, MNRAS, 282, 263
- Font A. S., Navarro J. F., Stadel J., Quinn T., 2001, ApJ, 563, L1
- Gao L., White S. D. M., Jenkins A., Stoehr F., Springel V., 2004, submitted to MNRAS (astro-ph/0404589)
- Ghigna S., Moore B., Governato F., Lake G., Quinn T., Stadel J., 1998, MNRAS, 300, 146
- Jenkins A., Frenk C. S., Pearce F. R., Thomas P. A., Colberg J. M., White S. D. M., Couchman H. M. P., Peacock J. A., Efstathiou G., Nelson A. H., 1998, ApJ, 499, 20
- Jenkins A., Frenk C. S., White S. D. M., Colberg J. M., Cole S., Evrard A. E., Couchman H. M. P., Yoshida N., 2001, MNRAS, 321, 372
- Kauffmann G., Colberg J. M., Diaferio A., White S. D. M., 1999, MNRAS, 303, 188
- Khochfar S., Burkert A., 2004, MNRAS submitted (astro-ph/0309611)
- Klypin A., Gottlöber S., Kravtsov A. V., Khokhlov A. M., ApJ, 516, 530
- Lacey C. G., Cole S., 1993, MNRAS, 262, 627
- Lacey C. G., Cole S., 1994, MNRAS, 271, 676
- Metcalf R. B., Madau P., 2001, ApJ, 563, 9
- Moore B., Lake G., Katz N., 1998, ApJ, 495, 139
- Moore B., Ghigna S., Governato F., Lake G., Quinn T., Stadel J., Tozzi P., 1999, ApJ, 524, 19
- Navarro J. F., Frenk C. S., White S. D. M., 1997, ApJ, 490, 493
- Peebles P. J. E., 1980, The Large Scale Structure of the Universe, Princeton Univ. Press, Princeton, NJ
- Taylor J. E., Babul A., 2001, MNRAS, 348, 811
- Tormen G., 1997, MNRAS, 290, 411
- Tormen G., Diaferio A., Syer D., 1998, MNRAS, 299, 728
- van den Bosch F. C., Lewis G. F., Lake G., Stadel J., 1999, ApJ, 515, 50
- Vitvitska M., Klypin A. A., Kravtsov A. V., Wechsler R. H., Primack J. R., Bullock J. S., 2002, ApJ, 581, 799
- Zhang B., Wyse R. F., Stiavelli M., Silk J., 2002, MNRAS, 332, 647